Intrinsic characteristics of semiconducting oxide nanobelt field-effect transistors

Yi Cheng and P. Xiong[a)]
Department of Physics, and MARTECH, Florida State University, Tallahassee, Florida 32306

Lenwood Fields and J. P. Zheng
Department of Electrical and Computer Engineering, FAMU/FSU College of Engineering, Tallahassee, Florida 32310

R. S. Yang and Z. L. Wang
School of Materials Science and Engineering, Georgia Institute of Technology, Atlanta, Georgia 30332

(Received 3 May 2006; accepted 2 July 2006; published online 30 August 2006)

Field-effect transistors (FETs) based on individual semiconducting oxide (SnO_2 and ZnO) nanobelts with multiterminal electrical contacts have been fabricated and characterized. Simultaneous two-terminal and four-terminal measurements enable direct correlation of the FET characteristics with the nature of the contacts. Devices with high-resistance non-Ohmic contacts exhibit a Schottky barrier FET behavior. In contrast, low-resistance Ohmic contacts on the nanobelt lead to high-performance *n*-channel depletion mode FETs with well-defined linear and saturation regimes, large "on" current, and an on/off ratio as high as 10^7. The FET characteristics of such devices show a significant modification by a 0.2% H_2 gas flow at room temperature. The excellent intrinsic characteristics of these nanobelt FETs make them ideal candidates as nanoscale biological and chemical sensors based on field-effect modulation of the channel conductance. © *2006 American Institute of Physics*. [DOI: 10.1063/1.2338754]

Various quasi-one-dimensional (1D) semiconductor nanostructures have received extensive recent interest,[1,2] due to their intrinsic nanoscale geometry and rich, sometimes unique, electrical, optical, and mechanical properties.[3] These nanocomponents can be produced in large quantities with physical or chemical vapor deposition techniques, and individual nanowires can be readily utilized to construct nanoscale functional devices. One class of device structures which has received particular attention are field-effect transistors (FETs). While some semiconductor nanowire-based FETs have shown promise as high-performance building blocks for future nanoelectronics,[4] the more immediate applications are likely to be in the arena of ultrasensitive chemical and biological sensing using individual or small arrays of nano-FETs.[5]

Semiconducting binary metal oxides have long been a class of technologically important sensor materials.[6] Recently, a wide variety of single-crystalline, quasi-1D forms (nanobelts, nanorods, and nanowires) of ZnO, SnO_2, and In_2O_3 has been synthesized[1,7] and used to produce nanoscale FETs and demonstrate various types of gas sensing.[8] Improved sensitivity and response time compared to thin-film-based sensors, especially at room temperature, were reported. Most of the previous studies, however, were based on two-terminal devices. It is well known that the source/drain contacts could dominate the transistor action and sensing response when Schottky barriers are present at the contacts.[9] For quantitative and scalable sensing applications, it is important to establish that the signal comes predominantly from the modulation of the channel rather than the contacts. It is therefore necessary to carefully evaluate the origin of the FET action in these devices.

In this letter, we report on a study comparing the effects of Schottky contacts and low-resistance Ohmic contacts on the characteristics of SnO_2 and ZnO nanobelt FETs. We show that while a large modulation of the source-drain current by gating can be obtained in both cases, the FET source-drain current (*I*)-voltage (*V*) characteristics, transfer characteristics, and magnitude of the "on" current are distinctly different. We demonstrate a direct correlation between the different FET behaviors and the nature of the source-drain electrical contacts with the nanobelt channel using multiterminal devices and simultaneous two- and four-terminal measurements. Low-resistance Ohmic contacts on the SnO_2 and ZnO nanobelts lead to high-quality *n*-channel depletion mode FETs with well-defined linear and saturation regimes, large on current, and on/off ratio as high as 10^7.

The SnO_2 and ZnO nanobelts were synthesized by thermal evaporation of pure oxide powders under controlled conditions without any catalyst.[1] The as-synthesized nanobelts are pure, single crystalline, and structurally uniform. They have a rectangularlike cross section with a typical thickness of tens of nanometers and width-to-thickness ratio of 5–10. Bundles of nanobelts retrieved from the alumina substrate were separated into individual nanobelts in an isopropanol solution by ultrasonic agitation, and then dispersed onto a substrate. An individual nanobelt was located and multiple electrodes were defined via photolithography, pulsed laser ablation and/or thermal evaporation, and lift-off. A *n*-type degenerately doped (100) Si substrate ($\rho \sim 1 m\Omega$ cm, $n \sim 10^{19}$ cm^{-3}) was used as a back gate, and a 250 nm thick thermally grown SiO_2 served as the insulating gate dielectric. All measurements were carried out in air at room temperature unless otherwise noted.

Low-resistance Ohmic contacts were realized on both SnO_2 and ZnO nanobelts and verified via direct comparison

[a)]Electronic mail: xiong@martech.fsu.edu

 © 2006 American Institute of Physics
Downloaded 05 Sep 2006 to 130.207.165.29. Redistribution subject to AIP license or copyright, see http://apl.aip.org/apl/copyright.jsp

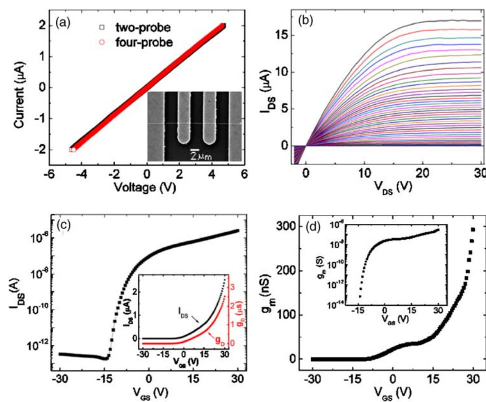

FIG. 1. (Color online) (a) Four-probe (red circle) and two-probe (black square) *I-V* curves of a SnO_2 nanobelt device with RuO_2/Au contacts. Inset: SEM micrograph of the device. (b) Source-drain *I-V* characteristics of the SnO_2 nanobelt FET at increasing gate voltage (−30 to +30 V) in steps of 1 V from bottom to top. (c) Transfer characteristics of the SnO_2 nanobelt FET at $V_{DS}=1$ V. Inset: Linear plots of $I_{DS}-V_{GS}$ and g_D-V_{GS} at $V_{DS}=1$ V. (d) Transconductance of the device at $V_{DS}=1$ V. Inset: Semilog plot of g_m-V_{GS} at $V_{DS}=1$ V.

of two-probe and four-probe *I-V* measurements. In order to achieve low-resistance Ohmic contacts *consistently* on SnO_2 nanobelts, we used pulsed laser deposition to deposit a coating of metallic RuO_2 (~200 nm) at room temperature, followed by a layer of Au (~100 nm) by thermal evaporation in order to ease wire bonding. Figure 1(a) shows the four-probe and two-probe (two center contacts) *I-V* characteristics of a SnO_2 nanobelt device with four RuO_2/Au contacts, as shown in the scanning electron microscopy (SEM) image in the inset. Both *I-V* curves are linear and the contact resistance is less than 1% of the channel resistance. The consistent formation of Ohmic contacts here is likely due to the limitation of interfacial diffusion and reaction at the SnO_2/RuO_2 interface. In contrast, direct metallization with Cr/Au and especially Ti/Au on SnO_2 nanobelts often results in poor electrical contacts. For ZnO nanobelts, Ti/Au metallization showed a high degree of reliability in producing low-resistance Ohmic contacts, although in some rare cases Schottky contacts were observed. Cr/Au, on the other hand, often lead to non-Ohmic contacts on ZnO nanobelts.

The nature of the contacts has a significant impact on the FET characteristics of the nanobelt devices. Figures 1(b)–1(d) display the room temperature FET behavior of the device shown in Fig. 1(a). The two middle leads were used as the source and drain electrodes. Since the contact resistance was determined to be at least two orders of magnitude smaller than the channel resistance, the measured FET characteristics reflect the intrinsic response of the SnO_2 channel. Figure 1(b) shows the source-drain *I-V* curves at various gate voltages from −30 to +30 V in steps of 1 V. In the on state, the *I-V* curves have a well-defined linear regime at low biases, and the drain current saturates upon further increase in the bias. The saturation behavior is similar to the pinch-off effect in conventional silicon FETs due to a local depletion of carriers around the drain electrode. The channel can be turned off with a negative gate voltage of −14 V, which is demonstrated more clearly in the transfer characteristic shown in Fig. 1(c). The I_{DS} vs V_{GS} plot in semilogarithmic scale at a constant $V_{DS}=1$ V (in the linear regime of the source-drain *I-V*) shows clearly a threshold voltage of −14 V and on/off ratio as large as 10^7. The inset of Fig. 1(c) shows

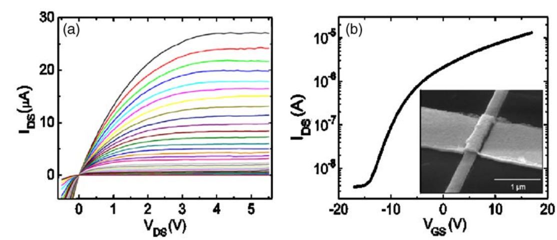

FIG. 2. (Color online) *n*-channel depletion mode FET based on a ZnO nanobelt: (a) I_{DS} vs V_{DS} at different gate voltages (V_{GS}) in steps of 1 V from −17 V (bottom) to +17 V (top). (b) Transfer characteristics of the FET at $V_{DS}=0.3$ V. Inset: A SEM image of the ZnO nanobelt contacted by a Ti/Au electrode.

that I_{DS} and conductance $g_D=\partial I_{DS}/\partial V_{DS}|_{V_G=\mathrm{const}}$ increase with increasing gate bias and reach their maximum values of 2.5 μA and 2.5 μS, respectively. The FET has an "off" state current of $\sim 10^{-13}$ A, which remains constant below V_{th}. The typical gate leakage current is measured to be at least two orders of magnitude smaller than I_{DS} in the off state and is gate bias independent. The subthreshold swing,[10] $S=\partial V_{GS}/\partial \log(I_{DS})$, is 1.02 V/decade for this device. Although for conventional Si metal-oxide-semiconductor field-effect transistor, the typical S value is 70–100 mV/decade, the subthreshold swing in our devices can be easily improved by reducing the thickness of the gate oxide layer (250 nm SiO_2 was used). Figure 1(d) and the inset show the transconductance, $g_m=\partial I_{DS}/\partial V_{GS}$, at $V_{DS}=1$ V in the same range of gate voltages. The effective field-effect carrier mobility μ_{eff} of the FET can be estimated[10] by $g_m=Z\mu_{eff}C_O V_{DS}/L$, where Z is the channel width (corresponding to the nanobelt width of 150 nm), L the channel length (corresponding to the electrode separation of 4 μm), and C_O the oxide capacitance per unit area (for the 250 nm thick SiO_2 substrate, $C_O=1.4\times 10^{-4}$ F/m^2). μ_{eff} shows a maximum value of around 334cm^2/V s at $V_{GS}=30$ V and a value of 26.1 cm^2/V s at $V_{GS}=0$ V. We emphasize that since the FET action in the device is channel limited, the calculated mobility is intrinsic to the SnO_2 nanobelt. The device also showed an excellent stability. Measurements before and after six month storage in ambient air yielded the same transistor behavior with identical transfer characteristics and consistent transconductance values.

Figure 2 shows the FET characteristics of a similarly constructed ZnO nanobelt device with Ti/Au Ohmic contacts. Compared with the SnO_2 nanobelts, the ZnO nanobelts are normally wider [a close-up view of the device is shown in the inset of Fig. 2(a)] and less resistive. While these differences lead to some modification of the details of the FET characteristics of the ZnO nanobelt device, the overall behavior remains similar to that of the SnO_2 FET. The source-drain *I-V* curves show well-defined linear and saturation regimes [Fig. 2(a)]; $I_{DS}-V_{GS}$ and g_D-V_{GS} at a drain bias of 0.3 V [Fig. 2(b) and the inset] show a threshold voltage of −14 V, maximum conductance of 18 μS, and on/off ratio approaching 10^4. The calculated effective mobility peaks at $\sim 1.35\times 10^3$ cm^2/V s at $V_{GS}=17$ V and is 4.40×10^2 cm^2/V s at $V_{GS}=0$ V, which is significantly larger than that in the ZnO thin film FETs.[11]

The electrical characteristics and performance of the FET devices are sensitively dependent upon the nature of the electrical contacts to the nanobelts. The source-drain *I-V* characteristics of a ZnO nanobelt device with non-Ohmic

Downloaded 05 Sep 2006 to 130.207.165.29. Redistribution subject to AIP license or copyright, see http://apl.aip.org/apl/copyright.jsp

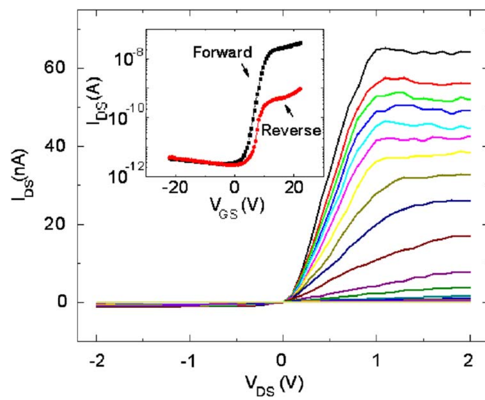

FIG. 3. (Color online) ZnO nanobelt asymmetric Schottky barrier FET: (a) $I_{DS}-V_{DS}$ plot with V_{GS} from −22 to 22 V in steps of 1 V. Inset: *n*-channel enhancement mode transfer characteristics of the FET in forward (V_{DS}= +0.5 V) and reverse (V_{DS}=−0.5 V) directions.

Cr/Au contacts are shown in Fig. 3. The source-drain *I-V* at $V_{GS}=0$ shows a strong rectifying behavior, clearly indicating Schottky source-drain contacts of different barrier heights. $I_{DS}-V_{DS}$ at different V_{GS} (from +22 to −22 V in steps of 1 V) shows a large gate modulation typical of a directionally dependent Schottky barrier FET. The inset shows the transfer characteristics at drain biases of $V_{DS}=+0.5$ and −0.5 V. In the forward direction, the maximum conductance g_D of the on state is about 7×10^{-7} S and the off state is $\sim10^{-12}$ S, with an on/off ratio greater than 10^4. The maximum transconductance g_m is about 10^{-8} S. In the reverse direction, these parameters are suppressed by more than two orders of magnitude. The directionally dependent behavior of the ZnO nanobelt FET closely resembles that in an intentionally fabricated asymmetrical carbon nanotube FET with one Ohmic contact and one Schottky contact.[12] Clearly, in this device the FET behavior is determined predominantly by one contact. A similar rectifying behavior was recently reported in ZnO nanobelt devices with structurally symmetrical contacts.[13] In our case, the characteristics of these nanobelt Schottky barrier FETs showed large variations in the degree of asymmetry and gate modulation from device to device. This is in contrast to the channel-limited nanobelt FETs with Ohmic contacts in which the FET characteristics are highly systematic and reproducible. These observations can be attributed to the fact that the Schottky barrier formation here is due to surface states.[14] Although the Schottky barrier FETs may have some advantages over normal FETs in certain electronics applications, precise control and reproducibility of the Schottky barrier contacts must first be obtained. Most importantly, for quantitative and scalable sensing applications with the nano-FETs, it is necessary to clearly establish that the FET action is from the channel rather than the contacts.

With clear identification of the channel-limited nanobelt FETs, we are able to evaluate the potential of the devices for sensor applications by examining the intrinsic response of the nanobelt channels. We have carried out a systematic study of the response of a channel-limited SnO_2 nanobelt FET (with RuO_2/Au contacts) to 0.2% H_2 balanced with N_2 at room temperature. Figures 4(a) and 4(b) show two series of $I_{DS}-V_{DS}$ plots in ambient air and in 0.2% H_2, respectively, at different gate voltages (−30 to +30 V). The FET characteristics show a significant modification upon exposure to

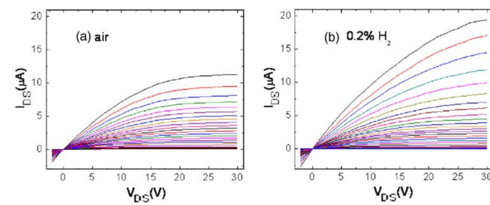

FIG. 4. (Color online) $I_{DS}-V_{DS}$ at various gate voltages (−30 to+30 V) in steps of 2 V for a SnO_2 nanobelt FET with Ohmic RuO_2/Au contacts (a) in air and (b) in 0.2% H_2 balanced with N_2 at room temperature.

0.2% H_2. The channel conductance (in the linear regime) increases by around 17% at all gate voltages. The hydrogen reacts with and removes the oxygen adsorbed on the metal oxide surface and thus increases the electron concentration and the conductance of the nanobelt channel. This also makes the pinchoff at the drain contact more difficult, which is evidenced by the fact that the linear region in the $I_{DS}-V_{DS}$ now extends to much higher drain biases. The dramatic response of the SnO_2 nanobelt FET to hydrogen at room temperature without any catalyst demonstrates great promise of such devices in chemical gas sensing under ambient conditions. Details of the hydrogen sensing experiments and results are described elsewhere.[15]

This work was supported by NSF NIRT Grant No. ECS-0210332 and a FSU Research Foundation PEG grant.

[1] Z. W. Pan, Z. R. Dai, and Z. L. Wang, Science **291**, 1947 (2001).
[2] Y. Wu, J. Xiang, C. Yang, W. Lu, and C. M. Lieber, Nature (London) **430**, 61 (2004); X. F. Duan, C. M. Niu, V. Sahi, J. Chen, J. W. Parce, S. Empedocles, and J. L. Goldman, *ibid.* **425**, 274 (2003).
[3] H. Kind, H. Yan, B. Messer, M. Law, and P. D. Yang, Adv. Mater. (Weinheim, Ger.) **14**, 158 (2002); M. Arnold, P. Avouris, Z. W. Pan, and Z. L. Wang, J. Phys. Chem. B **107**, 659 (2003); W. Hughes and Z. L. Wang, Appl. Phys. Lett. **82**, 2886 (2003).
[4] X. Duan, Y. Huang, Y. Cui, and C. M. Lieber, in *Molecular Nanoelectronics*, edited by M. A. Reed and T. Lee (American Scientific, Stevenson Ranch, CA, 2003), pp. 199–227.
[5] J. Kong, N. R. Franklin, C. Zhou, M. G. Chapline, S. Peng, K. Cho, and H. Dai, Science **287**, 622 (2000); F. Patolsky, G. Zheng, O. Hayden, M. Lakadamyali, X. Zhuang, and C. M. Lieber, Proc. Natl. Acad. Sci. U.S.A. **101**, 14017 (2004).
[6] T. Minami, MRS Bull. **25**, 38 (2000).
[7] Z. L. Wang and Z. W. Pan, Int. J. Nanosci. **1**, 41 (2002); Y. W. Heo, V. Varadarajan, M. Kaufman, K. Kim, D. P. Norton, F. Ren, and P. H. Fleming, Appl. Phys. Lett. **81**, 3046 (2002); P. D. Yang, H. Q. Yan, S. Mao, R. Russo, J. Johnson, R. Saykally, N. Morris, J. Pham, R. R. He, and H. J. Choi, Adv. Funct. Mater. **12**, 323 (2002).
[8] E. Comini, G. Faglia, G. Sberveglier, Z. Pan, and Z. L. Wang, Appl. Phys. Lett. **81**, 1869 (2002); C. Li, D. H. Zhang, X. L. Liu, S. Han, T. Tang, J. Han, and C. Zhou, *ibid.* **82**, 1613 (2003); Z. Fan, D. Wang, P. C. Chang, W. Y. Tseng, and J. G. Lu, *ibid.* **85**, 5923 (2004); H. T. Wang, B. S. Kang, F. Ren, L. C. Tien, P. W. Sadik, D. P. Norton, and S. J. Pearton, *ibid.* **86**, 243503 (2005).
[9] S. Heinze, J. Tersoff, R. Martel, V. Derycke, J. Appenzeller, and Ph. Avouris, Phys. Rev. Lett. **89**, 106801 (2002).
[10] S. M. Sze, *Physics of Semiconductor Devices*, 2nd ed. (Wiley, New York, 2002), p. 191.
[11] R. L. Hoffman, B. J. Norris, and J. F. Wager, Appl. Phys. Lett. **82**, 733 (2003).
[12] M. H. Yang, K. B. K. Teo, W. I. Milne, and D. G. Hasko, Appl. Phys. Lett. **87**, 253116 (2005).
[13] C. S. Lao, J. Liu, P. Gao, L. Zhang, D. Davidovic, R. Tummala, and Z. L. Wang, Nano Lett. **6**, 263 (2006).
[14] J. Singh, *Semiconductor Devices: Basic Principles* (Wiley, New York, 2001), p. 228.
[15] L. L. Fields, J. P. Zheng, Y. Cheng, and P. Xiong, Appl. Phys. Lett. **88**, 263102 (2006).

Downloaded 05 Sep 2006 to 130.207.165.29. Redistribution subject to AIP license or copyright, see http://apl.aip.org/apl/copyright.jsp